# Structure of Rhodamine 6G−DNA Complexes from Molecular Dynamics Simulations

Anela Ivanova,† Grzegorz Jezierski, Egor Vladimirov, and Notker Rösch*

*Department Chemie, Theoretische Chemie, Technische Universität München, 85747 Garching, Germany*

*Received May 18, 2007; Revised Manuscript Received August 6, 2007*

Chromophore−DNA complexes are useful for understanding charge transport along $\pi$-stacks once their structural properties have been clarified. We studied two rhodamine 6G semicapping complexes with 15-mer B-DNA duplexes to determine the preferred orientation of the dye with respect to the neighboring base pair. For each of these systems, two distinct chromophore alignments were identified and quantified in terms of base-step parameters. The obtained geometries agree well with those derived from an NMR structure refinement of similar complexes. Cross-correlation analysis of the base-step parameters shows that slide and twist are highly interdependent during the structural transition from one conformation to the other.

## Introduction

Structures of chromophore−DNA complexes have been intensively studied in recent years,[1−5] because such assemblies may be useful for constructing novel nanoelectronic devices.[6] Oxidized and reduced DNA can result from photoinduced electron transfer, possibly along the $\pi$-stack of the DNA helix.[7] In this process, the external chromophore acts as the electron acceptor and DNA as the electron donor or vice versa.[7−9] The best-characterized DNA modifications in terms of (mostly) electron hole transfer and its dynamics result from precise positioning of the dye through covalent bonding to one or both of the DNA strands via various linkers (bridges), mostly $CH_2$ tethers.[3,4,8,10,11] The rate of electron transfer was found to be highly sensitive to the sequence of the nucleobases and especially the nearest or next-nearest neighbor nucleobase.[3,4] A major factor is the electronic coupling between the chromophore and the nearest part of a DNA base.[3a,4a,12] For hole transfer from the chromophore, the location of the nearest guanine is important as it is the easiest one to oxidize among the canonical nucleobases.[13] Therefore, information about the mutual alignment of the chromophore and neighboring base pairs is very important.

NMR spectroscopy is a powerful experimental technique for determining the structure of complex bioorganic molecules in aqueous solution.[14] From a simulation perspective, vital structural information can be obtained via force-field-based molecular dynamics (MD) simulations. Also, insight into energetics and dynamics of chromophore−DNA systems can be gained at the time scale of several nanoseconds.

Rhodamine 6G (R6G) is a dye frequently used as a semicapping charge injector into DNA.[15,16] It is a zwitterionic $\pi$-conjugated molecule (Figure 1a) that contains a positively charged xanthene ring that, after excitation, can act as electron hole donor to a base of the neighboring DNA duplex. Recently, the structures of several R6G−DNA complexes have been studied by two-dimensional NMR.[16b,c] Two different orientations of the dye with respect to the DNA base stack have been identified as well as a structural exchange between them on the NMR time scale.

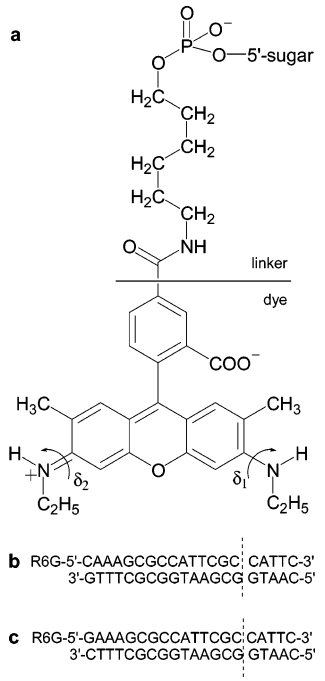


**Figure 1.** (a) Rhodamine 6G (R6G) with the aliphatic linker for binding to the DNA duplex (junction between R6G and linker indicated by a solid line). (b and c) Experimentally studied R6G−DNA complexes (NMR structure available for complex b). The dashed lines indicate the positions where the oligonucleotides were truncated to create the theoretical models R6G−CAA (modeling complex b) and R6G−GAA (modeling complex c).

Conformational variation of rhodamine binding to DNA was also reported in other studies.[15b,17,18] Vamosi et al. were the first to publish a very detailed fluorescence study on the binding of tetramethylrhodamine via a linker to a series of DNA duplexes.[15b] They discriminated three chemical species in their samples, exhibiting different patterns of interaction between rhodamine and DNA. Two of the states were fluorescent with significantly different fluorescence decay times (~0.7 and ~3.0 ns), and the third one was designated as a "dark state". Later on, Unruh et al. observed three different fluorescence decay times of the same

* Author to whom correspondence should be addressed. E-mail: roesch@ch.tum.de.

† On leave from the Department of Physical Chemistry, Faculty of Chemistry, University of Sofia, 1 J. Bourchier Avenue, 1164 Sofia, Bulgaria.

10.1021/bm700549g CCC: $37.00 
Published on Web 09/26/2007

dye bound to an aptamer at high temperature, which they related to a higher probability of two different conformations, as manifested by easier motion at an elevated temperature.[17a] They associated the two short decay times (0.14 and 0.63 ns) with electron transfer between the dye and the DNA while they related the long one (2.6 ns) to a geometric rearrangement of the N-alkyl substituents within the dye. On the basis of the three decay times, the authors estimated two rotational correlation times (corresponding most probably to two different rotations of the dye−aptamer system).[17b] The shorter rotational correlation time for the long-lived fluorescent state ranged up to 1.7 ns, and the longer one from 3 to 10 ns.

Similar fluorescence decay patterns were observed by von Feilitzsch.[16a] The resolved fluorescence decay times of the two fast components in one of the complexes under study were 0.18 and 0.63 ns, while the slow component, with a longer characteristic time of 4.1 ns, was assigned to a fraction of dyes that did not cap the duplex. The fluorescence anisotropy of the free dye decays monoexponentially within 0.2 ns, while the fluorescence anisotropy of an unquenched chromophore−DNA reference system decays biexponentially with characteristic times of 0.4 and 5 ns, assigned to DNA rotational relaxation.[16a]

The relative populations of the various rhodamine configurations on top of DNA stacks were found to depend on temperature,[15b,17] salt concentration, and concentration of ethanol[15b] but not on the length of the DNA duplex.[18] In spite of several models proposed to rationalize the conformational behavior of rhodamine bound to DNA,[15−18] many aspects remained unclear at the atomistic level.

To provide more insight into the molecular structure and the dynamics of the R6G−DNA systems studied by NMR and time-resolved fluorescence,[16] we carried out molecular dynamics simulations for two R6G−DNA complexes that are similar to those studied experimentally. We analyzed snapshots along the resulting trajectories to quantify the relative orientation of R6G with respect to the neighboring bases and compared the results to experimental data.[16] In this comparison, we used suitably generalized base-step parameters (three translational and three rotational) that are common for characterizing the local structure of DNA $\pi$-stacks.[19] With the help of a statistical analysis of the base-step parameters, we characterized the two distinct patterns of dye location with respect to its nearest neighboring bases.

## Molecular Models

The original dye molecule R6G has been modified, both for the experiments under discussion[16] and the present simulations, with an additional aliphatic linker, which allows its covalent attachment to one of the strands in the DNA stack (Figure 1a). In the fluorescence spectroscopic studies,[16b] R6G was attached to nine different DNA duplexes, but a full NMR structure was resolved for one R6G−DNA complex only,[16b] where rhodamine is bound to the 5′-end of a DNA duplex consisting of 20 base pairs (Figure 1b). The NMR structure refinement experiment revealed the coexistence of two substructures (Figure 2) of the R6G−DNA semicapping complex with different alignment of the dye "on top" of its neighboring base pair. In the structure with 20% amplitude, the dye is located primarily on top of the guanine base; the two aromatic planes are essentially screening each other (Figure 2b). In the more abundant structure, R6G occupies an intermediate position between guanine and cytosine (Figure 2a).

Kinetic and spectroscopic experiments were also carried out on R6G−DNA complex c (Figure 1c),[16a] but no NMR structural data are available. Complexes b and c (Figures 1b and 1c) differ only by the arrangement of the base pair adjacent to R6G. In complex c, the dye is attached to guanine, and cytosine is at the 3′-end of the complementary strand; i.e., the positions of guanine and cytosine are swapped with respect to complex b to allow a comparative study of R6G−guanine electronic coupling on the efficiency of hole transfer in the two systems.

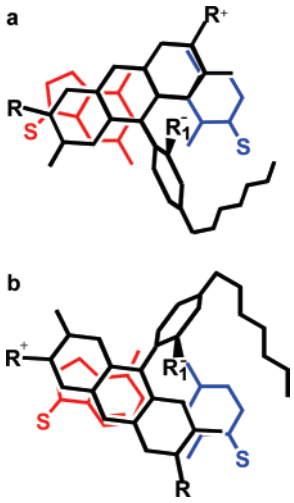


**Figure 2.** Schematic representation (view past the dye, along the $\pi$ stack of the oligomer) of the two NMR resolved substructures of the R6G−DNA complex shown in Figure 1b (adapted from ref 16b). Relative populations of conformations a/b in the experimental sample are 80%/20%: R, N-alkyl substituents; $R_1$, carboxy groups; S, sugar residue.

The MD simulations were performed for systems very similar to complexes b and c. The R6G−DNA sequences investigated theoretically are also indicated in Figures 1b and 1c. The only structural difference of the modeled complexes, R6G−CAA and R6G−GAA, from the experimental ones is that the DNA sequence is truncated after 15 base pairs (Figures 1b and 1c). In other words, the terminal five base pairs of the experimental DNA duplex were omitted for computational efficiency; still, these models are expected to essentially represent the structure and the electron-transfer properties of the systems studied experimentally.

## Computational Protocol

Molecular dynamics was chosen for the theoretical study because it allowed monitoring of the flexibility of the structure and permitted the detection and the quantification of the two substructures identified in the NMR experiment. The MD calculations were carried out with the program packages Amber 8[20] and NAMD 2.5.[21] The AMBER99 force field of Cornell et al. (ff99 parameter library) was used for DNA in all calculations,[22] because it affords an improved structural representation of DNA fragments due to torsional parameters. The gaff[23] force field parameters produced by module parmchk of Amber 8 were employed for the R6G molecule.

The gaff force field requires atomic charges to be provided for the calculation of the electrostatic contribution to the potential energy. The recommended strategy for acquiring appropriate atomic charges relies on the restrained electrostatic potential (RESP) scheme,[24] implemented in Amber 8, which consists of fitting atomic charges to the molecular electrostatic potential generated at the HF/6-31G* level. This scheme was used here to obtain RESP atomic charges for R6G. The geometries of the dye and the linker (terminated with a negatively charged methylphosphate group, required for subsequent attachment to DNA) were optimized separately at the B3LYP/6-31G* level using the program package Gaussian 03.[25] The structure of the linker was optimized in vacuum. To model the zwitterionic form of R6G, solvation in an aqueous medium was simulated with a polarizable continuum

**Table 1.** Size of the Simulated R6G−CAA and R6G−GAA Systems

| complex | no. of $Na^+$ | no. of $H_2O$ | total no. of atoms | box dimensions (Å) |
|---|---|---|---|---|
| R6G−CAA | 29 | 5192 | 16 635 | 51.0 × 49.6 × 88.2 |
| R6G−GAA | 29 | 4909 | 15 786 | 48.6 × 49.6 × 88.2 |

model.[26] A recent detailed study of this problem[27] provided evidence that the zwitterionic form becomes lower in energy than the lactone isomer only when solvation is adequately described.

After separate geometry optimization, the structures of the dye and linker were merged, and the electrostatic potential of the modified chromophore was generated at the RHF/6-31G* level,[24] using the program Gaussian 03. The calculated electrostatic potential was subjected to a RESP analysis using Amber 8 to generate the atomic charges for the modified R6G. The values used in the subsequent simulations are presented in Figure S1 of the Supporting Information. Cartesian coordinates of the two separate optimized molecules (dye and linker) as well as those of the merged structure are also provided (Tables S1−S3 of the Supporting Information).

The initial structures of the DNA duplexes were constructed with the program NAB[28] in B-DNA form in accordance with experiment.[16] The dye was attached to the corresponding DNA nucleotide. Sodium cations were used to neutralize the phosphate charges. This chromophore−DNA complex was solvated in TIP3P water[29] and enclosed in a rectangular periodic box, which was taken to extend about 10 Å from the solute in each direction. Force field parameters, topology, and Cartesian coordinates of the resulting structures were obtained with the LEaP module of Amber 8. Table 1 shows details related to the sizes of the simulated systems.

The MD trajectory of R6G−CAA was generated with Amber 8, and that of R6G−GAA with NAMD 2.5. Before running MD simulations, each initial structure was subjected to an equilibration procedure.[30] After 5000 steps of conjugate gradient energy minimization, the equilibration stage of the MD calculation for R6G−CAA consisted of heating the system from 0 to 298 K over 50 ps, employing an NVT ensemble, and then the MD calculation continued for additional 750 ps at 298 K. Analysis of that trajectory showed that the system was equilibrated already after 150 ps. Therefore, the preparation stage of R6G−GAA was shortened to 20 ps of heating from 2 to 298 K and 130 ps of equilibration at 298 K.

For each system, equilibration was followed by MD production runs of 10 ns using an NPT ensemble at 298 K and a pressure of 1 atm. In all MD simulations the particle mesh Ewald (PME) technique[31] was used to estimate the electrostatic interactions. A cutoff of 10 Å was applied to the direct part of the PME sum and when evaluating nonbonded interactions. All hydrogen-containing bonds were constrained with the SHAKE algorithm.[32] Standard AMBER99 scaling factors were invoked for 1−4 electrostatic and nonbonded interactions. Time steps of 2 fs were used. To verify the stability of the MD simulations, we monitored the fluctuations of the total energy, density of the system, temperature, and pressure.

Pertinent quantities of each trajectory, for R6G−CAA and R6G−GAA, were statistically analyzed for ensembles of 10 000 snapshots that had been extracted from the corresponding trajectories at intervals of 1 ps. To quantify the alignment of rhodamine 6G with respect to the adjacent guanine−cytosine (G−C) base pair of the DNA duplex, we introduced a generalization of the six "base-step" parameters (Figure 3), which were originally developed for pure DNA duplexes.[33] These parameters comprise three translations (shift, slide, and rise) and three rotations (tilt, roll, and twist), which completely describe the mutual orientation of two stacked rigid moieties. The generalized algorithm[34] for estimating the base-step parameters between R6G and its adjacent base pair G−C (or C−G) is similar to that employed in the program 3DNA.[35]

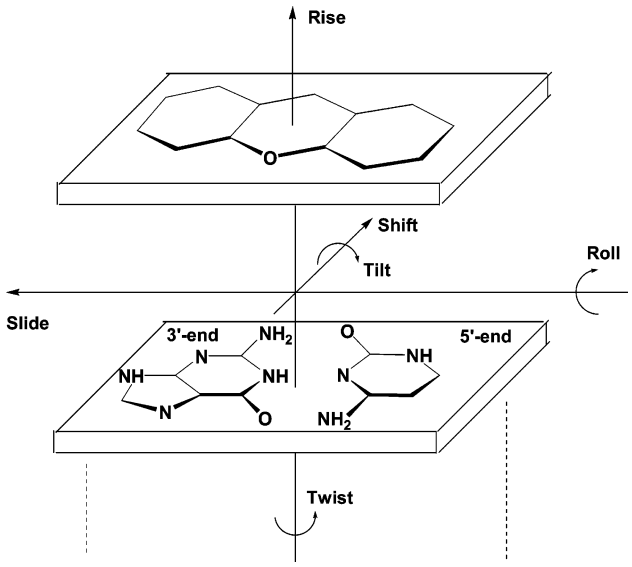


**Figure 3.** Coordinate system and designation of the six base-step parameters characterizing the position of the dye relative to the first base pair, illustrated for the example of R6G−CAA. The molecular planes of the dye and base pair are assumed to be parallel in terms of the three rotations. Arrows indicate positive directions of the translations (rotations).

## Results and Discussion

**Base-Step Parameters for R6G−CAA and R6G−GAA along Trajectories.** Figure 4 shows how the six base-step parameters between R6G and the adjacent G−C (or C−G) base pair evolve during 10 ns of simulation of the chromophore−DNA complexes R6G−CAA and R6G−GAA. Corresponding average values at batches of 1 ns and their standard deviations can be found in Table S4 of the Supporting Information.

The data for R6G−CAA in Figure 4 and Table S4 of the Supporting Information show that up to 4.5 ns rise, tilt, and roll are essentially stable, while shift, slide, and twist fluctuate more strongly. The standard deviations are relatively stable except for twist. The values of roll are larger than those of tilt, but the mean plane of R6G and the mean plane of the base pair remain essentially parallel. Yet, twist angles of about −50° imply that the two $\pi$ systems only have a partial overlap. The values of rise, the distance between the two molecular planes, are larger than those normally found between base pairs of DNA: ~3.7 Å in R6G−CAA versus 3.4 Å in similar simulations of a B-DNA duplex.[30] This enlarged average distance likely is due to the bulky substituents of the xanthene ring of R6G (see below). Nevertheless, the separation of R6G from the bases is still a typical stacking distance between two planar aromatic molecules. The absolute values of both shift and slide are close to 1 Å, but shift is negative and slide is positive. In other words, R6G is displaced in the direction of guanine, and the two molecules are overlapping each other to a large extent.

After 4.5 ns, all six base-step parameters of R6G−CAA change notably—a clear indication for a transition to a substantially different conformation. The most pronounced change occurs for twist, yet shift and slide also vary considerably. The other three parameters change as well but not dramatically. Twist, tilt, slide, and rise decrease, while roll and shift increase. Shift and slide change their sign; thus, the dye is displaced toward cytosine. The large negative value of twist in the second part of the R6G−CAA trajectory indicates that the dye adopts an almost antiparallel orientation with respect to the standard

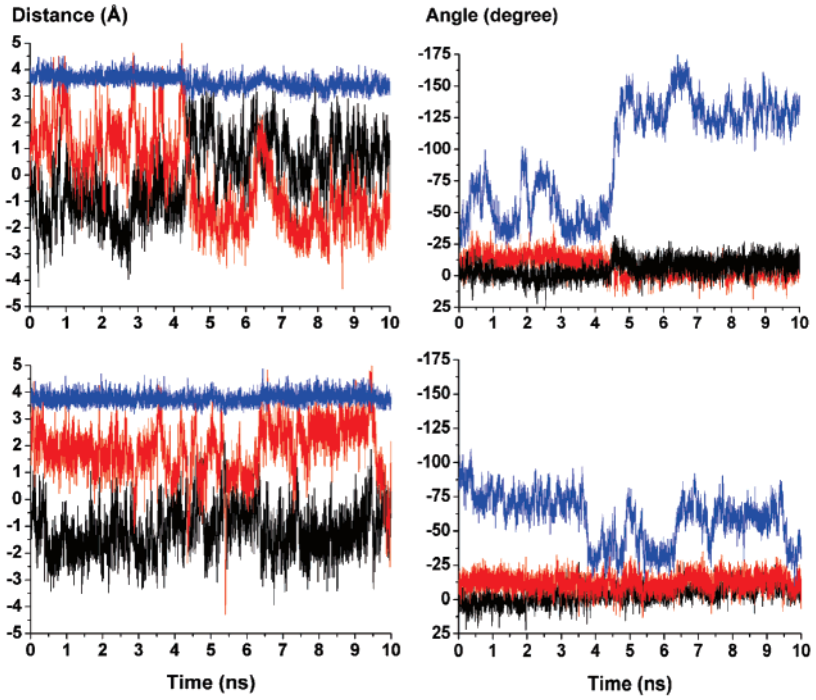


**Figure 4.** Evolution of the base-step parameters between the dye R6G and its neighboring G−C base pair for the complexes R6G−CAA (top) and R6G−GAA (bottom) from a MD trajectory of 10 ns. Left-hand panels: rise, blue; slide, red; shift, black. Right-hand panels: twist, blue; roll, red; tilt, black.

orientation of the G−C base pair, which is shown in Figure 3. The angle between the R6G plane and the plane of the base pair, reflected by tilt and roll, remains comparable to that in the first part of the trajectory because the two angles change by a comparable amount, but the values do not change their sign. On average, tilt becomes ∼7° more negative, and roll becomes ∼11° less negative. The smaller average of rise over the last 5 ns of the trajectory, ∼3.4 Å, may be due to an altered conformation of the ethyl substituents attached to xanthene nitrogen atoms. This smaller value of the rise is quite similar to that in pure DNA duplexes.

Analysis of the dihedral angles $\delta_1$ and $\delta_2$ (Figure 1a) shows that randomly in the entire trajectory about 75% of the structures feature ethyl substituents that both point away from the base pair; therefore, this structural aspect cannot be the reason for the different stacking in the two parts of the trajectory. The phenylcarboxy fragment of R6G is another part of the dye that prevents tighter packing with the adjacent $\pi$ system. In the initial part of the trajectory that group is oriented almost perpendicular to cytosine, preventing efficient hydrophobic interactions between the conjugated rings. However, upon the structural rearrangement, the phenylcarboxy moiety is placed in very close contact with the sugar residue that is attached to cytosine. Because the latter is more flexible than the base and can adjust its structure to relieve the strain, this allows more efficient stacking of the conjugated moieties, as is reflected in the smaller average value of rise (see above).

In summary, the major change of the base-step parameters observed in R6G−CAA between 4 and 5 ns signals a major reorientation of the dye with respect to the adjacent base pair.

Some general trends along the trajectory for the second system, R6G−GAA, remain similar to those along that of R6G−CAA. Rise, tilt, and roll are relatively stable throughout the entire simulation while shift, slide, and twist fluctuate more. The standard deviations of the corresponding parameters in the two systems are also similar. There is again a structural transition, after 3.6 ns, but in this case the changes are notably smaller than those for R6G−CAA. For example, in R6G−CAA twist changes by ∼125° between the two substructures, and in R6G−GAA the corresponding variation is ∼75°. In the latter complex, twist spans only the less negative values from the range of rotations observed for R6G−CAA. In other words, with respect to the neighboring base pair, the dye rotates from an almost parallel to a perpendicular orientation. In the beginning, the long axes of the dye and the base pair (Figure 3) are almost perpendicular to each other: Twist is about −90° (Figure 4). After the structural transition, the angle decreases to about −30°; i.e., the two step partners are aligned in a more parallel fashion. The values of shift and slide also change less during the structural transition of R6G−GAA. The negative values of shift and the positive values of slide in the first part of the trajectory imply that R6G is displaced in the direction of cytosine. During the rearrangement, the signs again revert, indicating a movement of the dye in the direction of guanine. With time, tilt becomes more negative, but its values are in the same range as those observed for R6G−CAA, from −25° to 10°. Rise is relatively large, which can be rationalized by the fact that in both substructures of R6G−GAA the phenylcarboxy fragment is located above guanine and thus prevents tight packing. As the transition between the two substructures of the complex does not affect rise, tilt, or roll in a notable manner, this structural rearrangement of the system has to be classified as much less severe than that in R6G−CAA.

Another important difference in the behavior of the two complexes is that, unlike R6G−CAA, R6G−GAA switches several times between the two sets of base-step parameters, remaining in the second substructure for a very short time only (less than 5% of the total trajectory; Figure 4).

Several snapshots from the MD trajectories (Figure 5) illustrate how the dye is placed relative to the adjacent G−C base pair. Four structures were selected from each trajectory as examples of the variation in base-step parameters. One notes that the orientation of the xanthene unit in the first part of the R6G−CAA trajectory (up to 4.5 ns) varies from a conformation

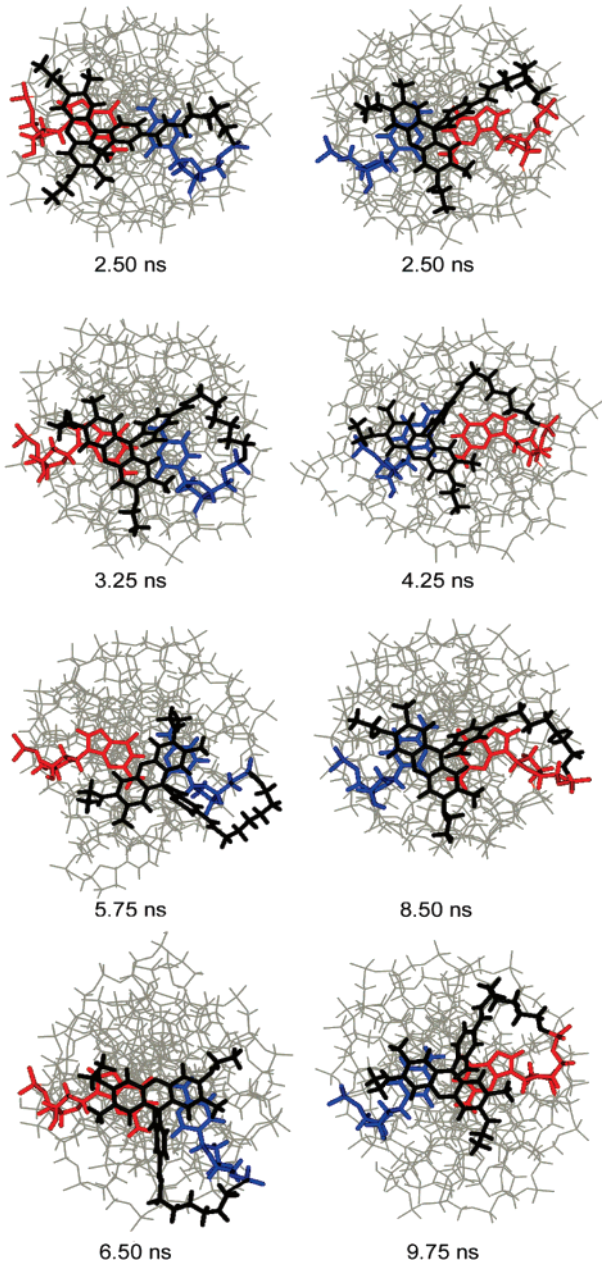


**Figure 5.** Snapshots (top view) of R6G−CAA (left-hand panels) and R6G−GAA (right-hand panels) illustrating the different relative positions of the dye R6G with respect to the neighboring G−C base pair. Color coding: R6G, black; cytidine, blue; guanidine, red; remaining DNA residues, light gray. Water molecules and sodium counterions omitted for clarity.

where the long axes of the two step partners are almost parallel to a conformation where these axes are almost perpendicular to each other; twist changes from about −30° to about −125°. However, the xanthene unit remains mostly on top of guanine, the overlap with cytosine being negligible. This alignment is similar to the minority NMR structure (20% amplitude; Figure 2b). In the R6G−CAA snapshots taken after the structural transition, the chromophore is almost equally spaced between guanine and cytosine. This alignment closely resembles the second, more abundant NMR structure (Figure 2a).

In R6G−GAA the separation of the two substructures is not so distinctive, but in general in the snapshots with larger twist the dye resides mostly on cytosine and in those with a smaller twist it is equally spaced from the centers of mass of the two adjacent bases. Only structures with highly negative values of slide (<−1.5 Å) correspond to a placement of R6G on top of guanine. Thus, observed also experimentally,[16] the abundance of the two substructures seems to depend on the immediate environment of the chromophore. In both R6G−CAA and R6G−GAA, those alignments in which R6G has appreciable interaction with cytosine are favored.

It is interesting to trace how the chromophore affects the structure of the adjacent part of DNA. Table S5 of the Supporting Information summarizes average values of base-step parameters estimated for the DNA steps 1−2 (CG,AT), 5−6 (GC,CG), 9−10 (CG,AT), and 14−15 (GC,CG) of the duplexes R6G−CAA and R6G−GAA. The numbers count the base pairs from the 5′-end of the strand to which R6G is attached. We chose these steps as pairs of identical types, 1−2 and 9−10 as well as 5−6 and 14−15, but one is located at the end of a duplex, and the other one has an internal position. The calculated average base-step parameters (BSPs) of the two types of steps fall within the range for the corresponding step as estimated from statistical analysis of X-ray structures.[36] In both systems, the standard deviations of all six parameters of the terminal step 1−2, capped by the dye, are similar to those of the corresponding internal steps. In contrast, the standard deviations of all BSPs of the GC terminal steps 14−15 at the uncapped duplex terminus of either system are larger than those of corresponding "internal" GC steps 5−6. Thus, taking the standard deviations of each BSP of terminal residues as indicators for the amount of fraying, then the presence of the dye indeed seems to reduce fraying of its neighboring base pair.

**Statistical Analysis of the Substructures Based on Calculated Base-Step Parameters.** To quantify the differences between the two distinct substructures of R6G−CAA and R6G−GAA in more detail, we carried out two types of statistical analysis.

The evolution of the calculated base-step parameters of R6G−CAA along the trajectory (Figure 4) seems to imply a concerted motion of R6G in three degrees of freedom: shift, slide, and twist. To corroborate this observation, we evaluated pairwise cross-correlation functions (CCFs)

$$\gamma(d) = (N-d)^{-1}(\sigma_x\sigma_y)^{-1}\sum_{t=1}^{N-d}(x_t-\bar{x})(y_{t+d}-\bar{y}) \qquad (1)$$

of these three parameters, using the utility xcor of the program package TISEAN.[37] In eq 1, $\gamma(d)$ is the cross-correlation function for lag $d$, $\sigma_x$ and $\sigma_y$ denote the standard deviations of the two data series $\{x_t\}$ and $\{y_t\}$, $\bar{x}$ and $\bar{y}$ are the corresponding average values, and $N$ is the number of points in each data set. Figure 6 shows the results for various series of snapshots from the MD trajectories of R6G−CAA and R6G−GAA.

The cross-correlation functions of the base-step parameters for the two complexes differ considerably. All three parameters are highly correlated for R6G−CAA, whereas for R6G−GAA a notable correlation is observed only between slide and twist. Correlation between the base-step parameters is indicated (i) by a nonzero average of each of the CCFs and (ii) by standard deviations larger than $(N-1)/2$. In R6G−CAA, shift exhibits analogous correlation patterns with slide and twist, and the latter two are oppositely correlated with each other; i.e., in the regions where shift is positively correlated with the other two parameters, they are negatively correlated with each other. None of the three base-step parameters is leading or lagging the other two as the CCF curves are symmetric with respect to a lag of 0 ns and have extremes at similar ranges of lags. This proves a concerted motion of the dye on top of the DNA duplex,

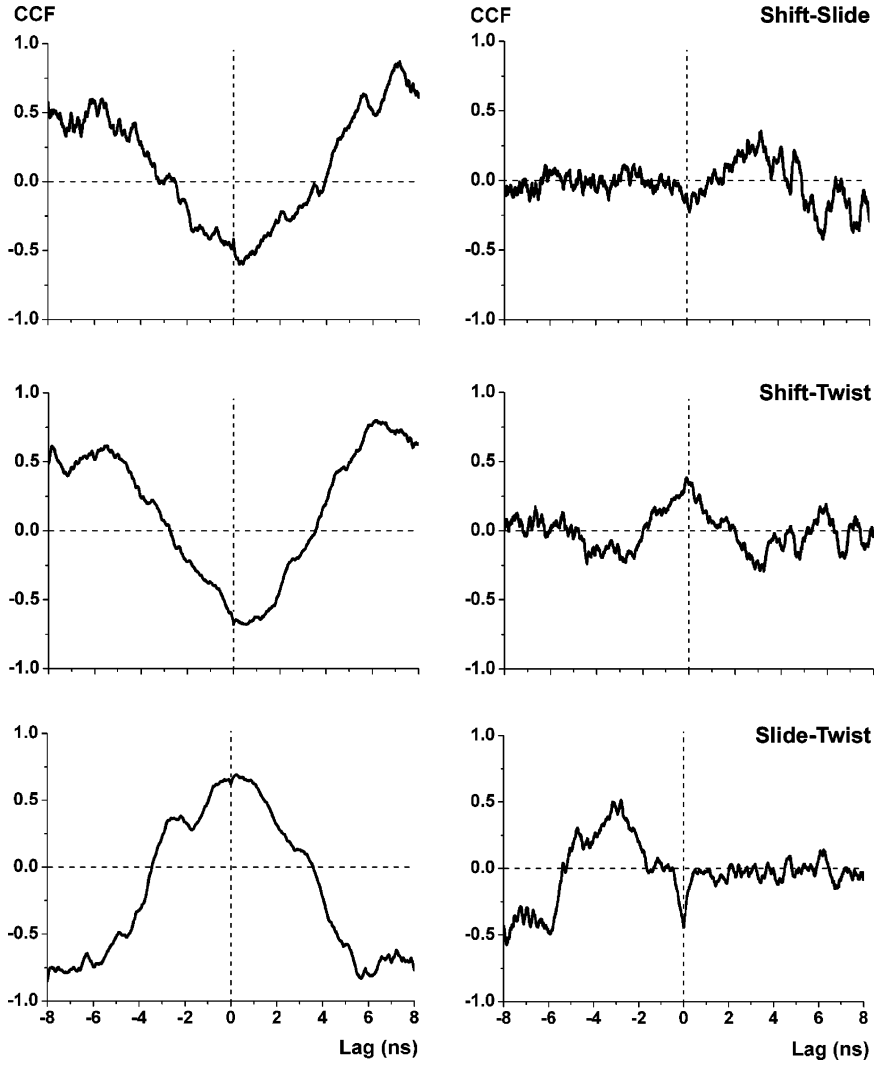


**Figure 6.** Cross-correlation functions (CCFs) of shift, slide, and twist between the dye R6G and the first base pair of the complexes R6G−CAA (left-hand panels) and R6G−GAA (right-hand panels) from a MD trajectory of 10 ns.

involving a synchronous variation in at least three degrees of freedom as expressed by the base-step parameters. In R6G−GAA, shift lacks a pronounced dependence on the other two variables. Slide and twist are correlated only at negative lag values. There, a change of twist precedes a change of slide. A positive value of lag implies the opposite.

A common feature of all of the cross-correlation functions shown in Figure 6 is that the character of correlation along the trajectory (as estimated from the zero-point crossings) changes from correlated to anticorrelated or vice versa. In R6G−CAA, a single crossing occurs at lag values between 3 and 4 ns. The first extremum of each CCF occurs at a very small value of lag (<0.5 ns); thus, a change in one of the three base-step parameters implies an almost immediate change of the other two. At lag values between 6 and 7 ns, each CCF reaches a second extremum but of opposite sign compared to the first one. This part of each CCF reflects the correlation of the two parts of the trajectory attributed to the different substructures. The large value of each CCF in this region thus indicates a well-defined structural correlation between the two substantially different substructures.

In contrast, multiple zero-point crossings appear in the CCFs of R6G−GAA. Extrema of opposite signs at lag values of about −3 and −7 ns can be identified only in the slide−twist CCF of R6G−GAA. Hence, twist is the leading degree of freedom in both substructures of the ensemble sampled. The extremum at the smaller lag values indicates a structural correlation between the two substructures of R6G−GAA.

The cross-correlation results obtained for shift, slide, and twist imply two distinct conformations, which should be manifested in two alignments of the dye relative to the adjacent base pair. This is confirmed by scatter plots of each pair of these three base-step parameters, which are presented in Figure 7.

The plots for shift−twist and slide−twist of the R6G−CAA complex clearly show a separation of pairs of parameters in two individual groups, which can be ascribed unequivocally to the existence of two substructures. The separation is not so clear in the shift−slide plot, where the two configuration regions are overlapping. The two different conformations can be distinguished most clearly by their twist angle where a twist value of about −100° represents a boundary, irrespective of the values of slide and shift.

In contrast, the scatter plots for R6G−GAA do not reveal any clear separation of the pairs of base-step parameters into groups. A very small "tail" is observed only in the graph of slide−twist; it represents a limited number of structures with negative slide and small values of twist. This is in line with the low population of the second substructure as induced from the changes of the base-step parameters along the trajectory of R6G−GAA (Figure 4).

To unravel the time evolution of the two substructures, we inspected scatter plots of shift, slide, and twist for subsequent

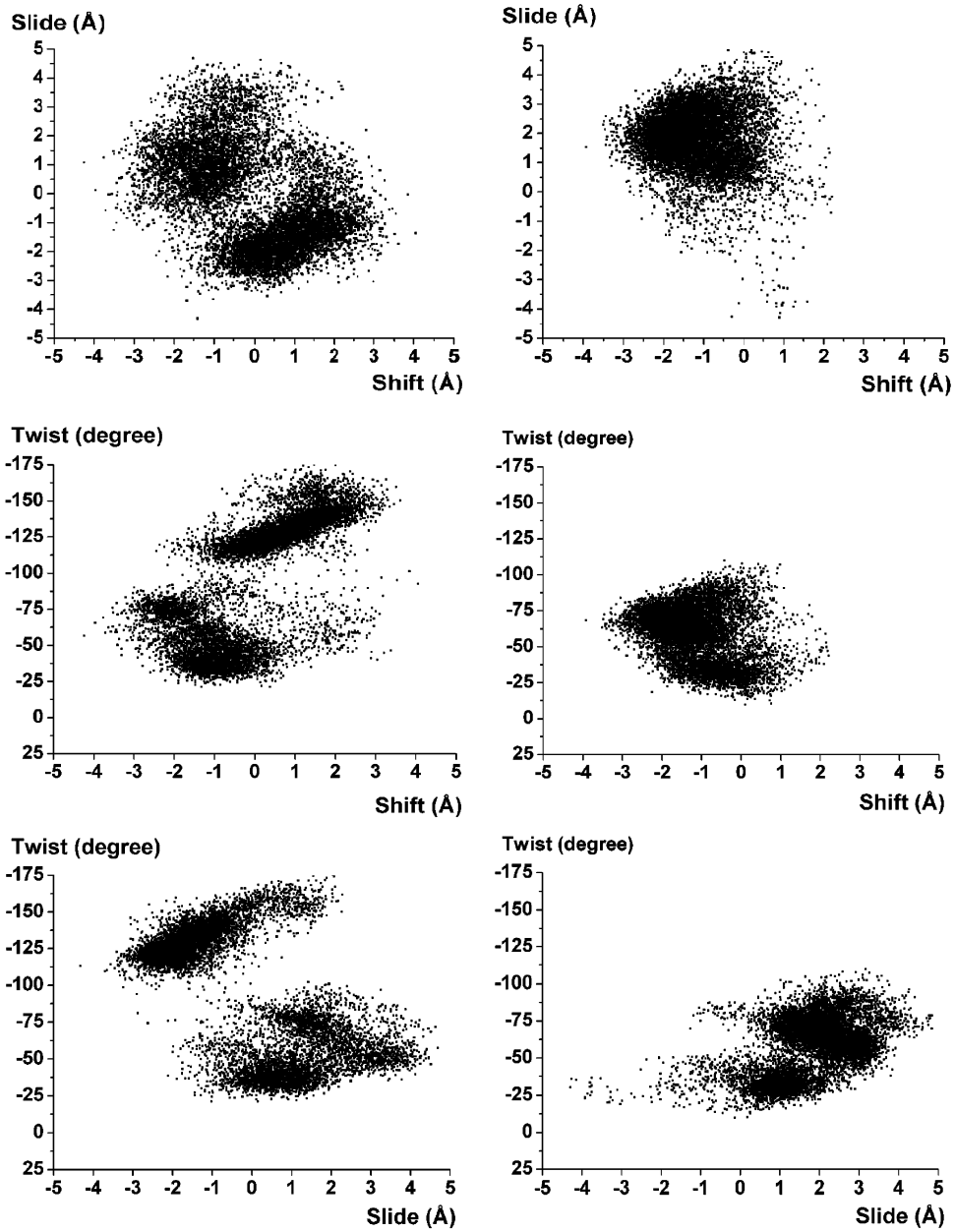


**Figure 7.** Scatter plots of shift, slide, and twist between the dye R6G and the first base pair of the complexes R6G−CAA (left-hand panels) and R6G−GAA (right-hand panels) extracted at 2 ps intervals from a MD trajectory of 10 ns.

intervals of 2 ns along the trajectories (Figures S2−S4 of the Supporting Information). Evidently, the two conformations of R6G−CAA are notably separated from both a static and a dynamic point of view. For 40% of the sampling time only one of the conformations is populated, then a qualitative change sets in, as a second conformation evolves. However, after 6 ns, only the second conformation survives. The presence of representatives of both types of conformations in the interval from 4 to 6 ns nicely corroborates the structure transition at ∼4.5 ns discussed above (Figure 4). A very similar behavior was registered for the three pairs of correlated parameters, even for slide and shift (Figure S2 of the Supporting Information), where the separation is not so evident from the overall scatter plot (Figure 7).

Also time-separated scatter plots of R6G−GAA do not clearly delineate the two conformations, but two subpopulations became apparent in the graphs for shift−twist (Figure S3 of the Supporting Information) and slide−twist (Figure S4 of the Supporting Information). Two conformational subsets can be distinguished in all graphs after 3 ns. The population of the structure with smaller twist values is lower in all time periods where it is observed.

The relative populations of the two substructures in the two trajectories can be quantified from a distribution analysis of the six base-step parameters (Figure 8). The widths of the bins are 1° for tilt and roll, 2° for twist, 0.1 Å for shift and slide, and 0.05 Å for rise.

Twist and slide of R6G−CAA exhibit apparently bimodal distributions. The other parameters show unimodal distributions, but all have certain degree of asymmetry with respect to the mean value. Therefore, they are probably bimodal as well, but the two subdistributions overlap. The distributions of R6G−GAA differ markedly from those of R6G−CAA. The base-step parameters of the former are again somewhat asymmetric, but only the distribution of twist is obviously bimodal. This finding agrees with the higher structural similarity of the two conformers of R6G−GAA.

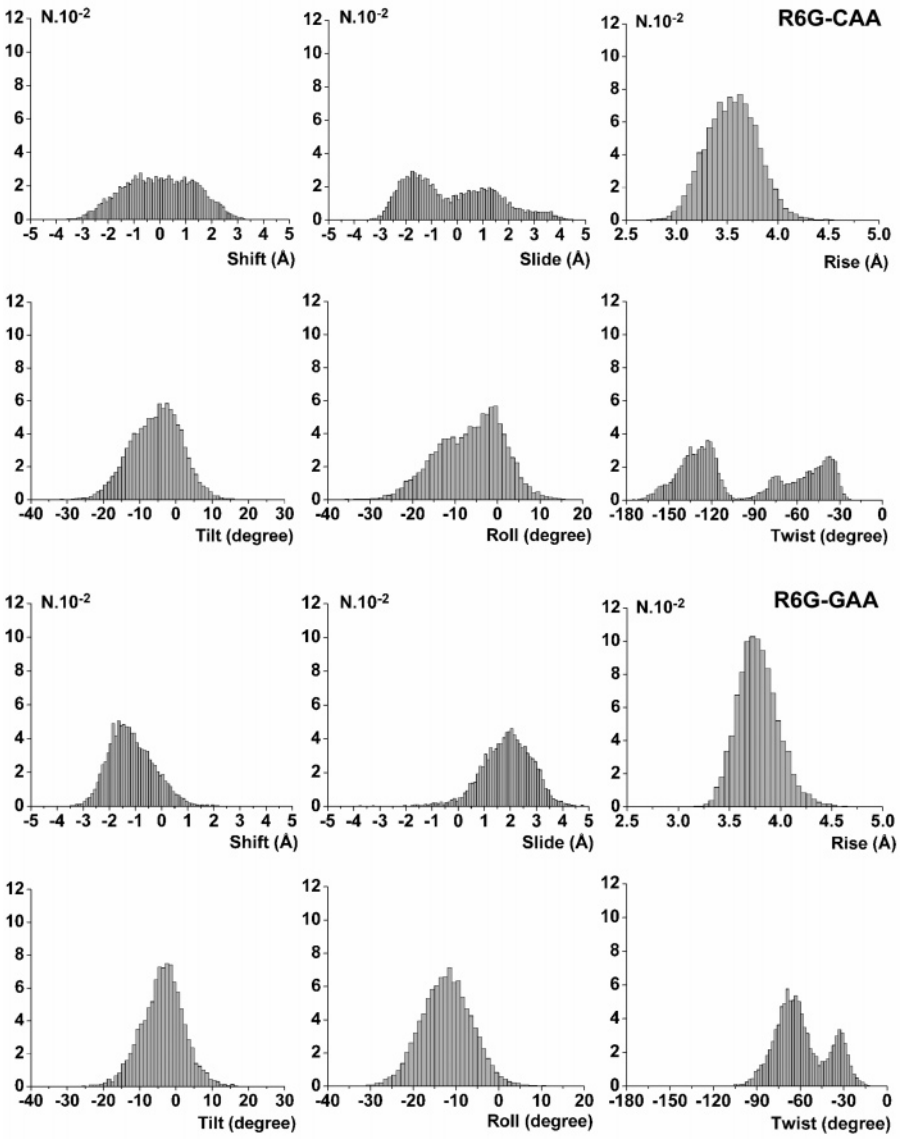


**Figure 8.** Distribution analysis of the base-step parameters between the dye R6G and the first base pair of the complexes R6G−CAA (top two rows) and R6G−GAA (bottom two rows) extracted at 1 ps intervals from a MD trajectory of 10 ns. *N* is the number of structures.

**Table 2.** Average Values and Standard Deviations of the Two Subdistributions for Twist, Roll, and Slide between R6G and the G−C Base Pair of R6G−CAA and for Twist of R6G−GAA, Based on the Distribution Analysis Shown in Figure 8

| complex | parameter | range | average | occurrence (%) |
|---|---|---|---|---|
| R6G−CAA | twist (deg) | −180 to −100 | −131.8 ± 13.0 | 54 |
| | | −100 to −20 | −21.1 ± 17.0 | 46 |
| | slide (Å) | −4.0 to −0.5 | −1.67 ± 0.62 | 51 |
| | | −0.5 to 5.0 | 1.25 ± 1.10 | 49 |
| | roll (deg) | −40 to −8 | −14.3 ± 4.6 | 44 |
| | | −8 to 20 | 1.2 ± 4.3 | 56 |
| R6G−GAA | twist (deg) | −110 to −48 | −68.2 ± 10.6 | 72 |
| | | −48 to 0 | −34.0 ± 6.9 | 28 |

On the basis of this distribution analysis, we calculated separate average values and standard deviations for the two subgroups of twist, roll, and slide of R6G−CAA and for twist of R6G−GAA (Table 2); we also present relative populations of the two conformers.

Inspection of Table 2 reveals that the structure during the second part of the R6G−CAA trajectory, characterized with more negative values of twist and slide, has a slightly larger population, although the probability ratio is not close to the experimental ratio of 4:1.[16b,c] Very likely, this fact is due to the limited time scale of the MD simulations, which are restricted to nanoseconds and therefore do not provide an adequate sampling of phase space in view of the fact that the two conformations seem to have life times of several nanoseconds. Recall that the NMR spectra were accumulated over intervals of several milliseconds.[16b,c] The corresponding distribution of the conformations of R6G−GAA is about 7:3 (Table 2). These results illustrate the finding that the relative populations of the two rhodamine orientations with respect to the neighboring base pair depend on the chemical nature of the underlying bases.[16] The set of base-step parameters corresponding to the more populated structure indicates that the dye preferentially interacts with cytosine.

The attractive interaction between the dye and the adjacent cytosine is of an electrostatic nature. As a rough measure for the charges of the various moieties, one may invoke sums of the corresponding RESP atomic charges used in the force field (Figure S1 of the Supporting Information). Accordingly, the substituted xanthene ring of rhodamine carries 0.90*e*, cytosine −0.66*e*, and guanine −0.09*e*. Thus, cytosine with its much more negative charge than guanine attracts the positively charged xanthene part of the dye more strongly.

The two differing sets of values of base-step parameters, observed for the complexes studied, very likely entail dissimilar electronic couplings between the dye and the adjacent base pair. Properly averaged quantum mechanical results are required to draw quantitative conclusions.

## Summary and Conclusions

Our molecular dynamics simulations on two semicapped chromophore−DNA complexes, R6G−CAA and R6G−GAA, in explicit water solvent, furnished clear evidence for two distinct conformations of the dye in relationship to its neighboring base pair.

This holds in particular for the complex R6G−CAA where the two conformations closely resemble the experimental NMR structures of a similar complex.[16b,c] Three base-step parameters—twist, slide, and shift—are most substantially affected during the transition between the two substructures, which, on the present trajectory, started at about 4.5 ns. In R6G−GAA**,** two conformations were registered as well, and the transition was found to be governed mostly by twist and slide. However, the transition took place earlier (at about 3.6 ns) and involved smaller structural rearrangement than in R6G−CAA; the less pronounced nature of the transition prevented a straightforward quantification. Moreover, the transition of R6G−GAA seems to be energetically more facile, as representatives of the two substructures were witnessed in various parts of the trajectory. This was different from the findings for R6G−CAA, where the two conformers are separated also in time. The observed characteristic times of dye rotation fall within the range of rotational correlation times determined from fluorescence spectroscopy measurements.[17b]

Clearly, for a more quantitative exploration of the phase space of such chromophore−DNA complexes free-energy calculations along paths in the space of base-step parameters are highly desirable.

**Acknowledgment.** The authors thank M.-E. Michel-Beyerle, T. von Feilitzsch, and C. Griesinger for valuable suggestions and helpful discussions. A.I. is grateful to the Alexander von Humboldt Foundation for a research fellowship. This work was supported by the European Union within the 6th Framework Program via the Specific Targeted Research Project No. NMP4-CT-2003-505669 (CIDNA), the Volkswagen Foundation (Project No. I/78 126), and the Fonds der Chemische Industrie.

**Supporting Information Available.** Cartesian coordinates (Tables S1−S3) and RESP atomic charges of R6G used in the simulations (Figure S1), base-step parameters averaged at 1 ns intervals of the MD trajectories for R6G−CAA and R6G−GAA (Table S4), average values of the base-step parameters of the (CG,AT) and (GC,CG) steps of the two DNA duplexes (Table S5), and scatter plots of shift, slide, and twist in the two complexes collected in 2 ns ranges during the molecular dynamics (Figures S2−S4). This material is available free of charge via the Internet at http://pubs.acs.org.

## References and Notes

(1) (a) Gasper, S. M.; Armitage, B.; Shui, X.; Hu, G. G.; Yu, C.; Schuster, G. B.; Williams, L. D. *J. Am. Chem. Soc.* **1998**, *120*, 12402−12409. (b) Trieb, M.; Rauch, C.; Wibowo, F. R.; Wellenzohn, B.; Liedl, K. R. *Nucleic Acids Res.* **2004**, *32*, 4696−4703. (c) Alexopoulos, E.; Jares-Erijman, E. A.; Jovin, T. M.; Klement, R.; Machinek, R.; Sheldrick, G. M.; Uson, I. *Acta Crystallogr., Sect. D: Biol. Crystallogr.* **2005**, *61*, 407−415.

(2) (a) Thornton, N. B.; Wojtowicz, H.; Netzel, T.; Dixon, D. W. *J. Phys. Chem. B* **1998**, *102*, 2101−2110. (b) Ohya, Y.; Yabuki, K.; Hashimoto, M.; Nakajima, A.; Ouchi, T. *Bioconjugate Chem.* **2003**, *14*, 1057−1066.

(3) (a) Lewis, F. D.; Kalgutkar, R. S.; Wu, Y.; Liu, X.; Liu, J.; Hayes, R. T.; Miller, S. E.; Wasielewski, M. R. *J. Am. Chem. Soc.* **2000**, *122*, 12346−12351. (b) Lewis, F. D.; Liu, J.; Zuo, X.; Hayes, R. T.; Wasielewski, M. R. *J. Am. Chem. Soc.* **2003**, *125*, 4850−4861.

(4) (a) Hess, S.; Götz, M.; Davis, W. B.; Michel-Beyerle, M.-E. *J. Am. Chem. Soc.* **2001**, *123*, 10046−10055. (b) Wagner, Th.; Davis, W. B.; Lorenz, K. B.; Michel-Beyerle, M. E.; Diederichsen, U. *Eur. J. Org. Chem.* **2003**, *18*, 3673−3679.

(5) Bloomfield, V. A.; Crothers, D. M.; Tinoco, I. *Nucleic Acids: Structures, Properties, and Functions*, University Science Books: Sausalito, CA, 1999.

(6) (a) Braun, E.; Eichen, Y.; Sivan, U.; Ben-Joseph, G. *Nature* **1998**, *391*, 775−778. (b) Fink, H.-W.; Schoenenberger, C. *Nature* **1999**, *398*, 407−410. (c) Porath, D.; Bezryadin, A.; De Vries, S.; Dekker, C. *Nature* **2000**, *403*, 635−638. (d) Adams, D. M.; Brus, L.; Chidsey, C. E. D.; Creager, S.; Creutz, C.; Kagan, C. R.; Kamat, P. V.; Lieberman, M.; Lindsay, S.; Marcus, R. A.; Metzger, R. M.; Michel-Beyerle, M. E.; Miller, J. R.; Newton, M. D.; Rolison, D. R.; Sankey, O.; Schanze, K. S.; Yardley, J.; Zhu, X. *J. Phys. Chem. B* **2003**, *107*, 6668−6697.

(7) (a) Meggers, E.; Michel-Beyerle, M. E.; Giese, B. *J. Am. Chem. Soc.* **1998**, *120*, 12950−12955. (b) Porath, D.; Cuniberti, G.; Di Felice, R. *Top. Curr. Chem.* **2004**, *237*, 183−227. (c) Giese, B. *Top. Curr. Chem.* **2004**, *236*, 27−44. (d) Lewis, F. D. *Photochem. Photobiol.* **2005**, *81*, 65−72.

(8) (a) Lewis, F. D.; Zhu, H.; Daublain, P.; Fiebig, T.; Raytchev, M.; Wang, Q.; Shafirovich, V. *J. Am. Chem. Soc.* **2006**, *128*, 791−800. (b) Lewis, F. D.; Zhu, H.; Daublain, P.; Cohen, B.; Wasielewski, M. R. *Angew. Chem., Int. Ed.* **2006**, *45*, 7982−7985.

(9) (a) *Photochemistry and the Nucleic Acids*; Morrison, H., Ed.; Bioorganic Photochemistry 1; Wiley: New York, 1990. (b) Adams, D. M.; Brus, L.; Chidsey, C. E. D.; Creager, S.; Creutz, C.; Kagan, C. R.; Kamat, P. V.; Lieberman, M.; Lindsay, S.; Marcus, R. A.; Metzger, R. M.; Michel-Beyerle, M. E.; Miller, J. R.; Newton, M. D.; Rolison, D. R.; Sankey, O.; Schanze, K. S.; Yardley, J.; Zhu, X. *J. Phys. Chem. B* **2003**, *107*, 6668−6697.

(10) (a) Fukui, K.; Morimoto, M.; Segawa, H.; Tanaka, K.; Shimidzu, T. *Bioconjugate Chem.* **1996**, *7*, 349−355. (b) Fukui, K.; Tanaka, K. *Angew. Chem.* **1998**, *110*, 167−170. (c) Gallego, J.; Reid, B. R. *Biochemistry* **1999**, *38*, 15104−15115. (d) Davis, W. B.; Hess, S.; Naydenova, I.; Haselsberger, R.; Ogrodnik, A.; Newton, M. D.; Michel-Beyerle, M.-E. *J. Am. Chem. Soc.* **2002**, *124*, 2422−2423. (e) von Feilitzsch, T.; Neubauer, H.; Griesinger, C.; Michel-Beyerle, M. E., to be submitted for publication.

(11) (a) Wan, C.; Fiebig, T.; Kelley, S. O.; Treadway, C. R.; Barton, J. K.; Zewail, A. H. *Proc. Natl. Acad. Sci. U.S.A.* **1999**, *96*, 6014−6019. (b) O'Neill, M.; Becker, H. C.; Wan, C.; Barton, J. K.; Zewail, A. H. *Angew. Chem., Int. Ed.* **2003**, *42*, 5896−5900.

(12) Beljonne, D.; Pourtois, G.; Ratner, M. A.; Bredas, J.-L. *J. Am. Chem. Soc.* **2003**, *125*, 14510−14517.

(13) (a) Seidel, C. A.; Schulz, A.; Sauer, M. H. M. *J. Phys. Chem.* **1996**, *100*, 5541−5553. (b) Voityuk, A. A.; Jortner, J.; Bixon, M.; Rösch, N. *Chem. Phys. Lett.* **2000**, *324*, 430−434.

(14) (a) Richter, C.; Reif, B.; Worner, K.; Quant, S.; Marino, J. P.; Engels, J. W.; Griesinger, C.; Schwalbe, H. *J. Biomol. NMR* **1998**, *12*, 223−230. (b) Bostock-Smith, C. E.; Laughton, C. A.; Searle, M. S. *Biochem. J.* **1999**, *342*, 125−132. (c) Bhattacharya, P. K.; Cha, J.; Barton, J. K. *Nucleic Acids Res.* **2002**, *30*, 4740−4750. (d) Arthanari, H.; McConnell, K. J.; Beger, R.; Young, M. A.; Beveridge, D. L.; Bolton, P. H. *Biopolymers* **2003**, *68*, 3−15. (e) van Buuren, B. N. M.; Schleucher, J.; Wittmann, V.; Griesinger, C.; Schwalbe, H.; Wijmenga, S. S. *Angew. Chem., Int. Ed.* **2004**, *43*, 187−192.

(15) (a) Mergny, J.-L.; Boutorine, A. S.; Garestier, T.; Belloc, F.; Rougee, M.; Bulychev, N. V.; Koshkin, A. A.; Bourson, J.; Lebedev, A. V.; Valeur, B.; Thuong, N. T.; Helene, C. *Nucleic Acids Res.* **1994**, *22*, 920−928. (b) Vamosi, G.; Gohlke, C.; Clegg, R. M. *Biophys. J.* **1996**, *71*, 972−994. (c) Seidel, C. A. M; Schulz, A.; Sauer, M. H. M. *J. Phys. Chem.* **1996**, *100*, 5541−5553. (d) Dietrich, A.; Buschmann, V.; Mueller, C.; Sauer, M. *Rev. Mol. Biotechnol.* **2003**, *82*, 211−231. (e) Heinlein, T.; Knemeyer, J.-P.; Piestert, O.; Sauer, M. *J. Phys. Chem. B* **2003**, *107*, 7957−7964.

(16) (a) von Feilitzsch, T. Dissertation, Technische Universität München, 2002. (b) Neubauer, H. Dissertation, Johann Wolfgang Goethe Universität Frankfurt am Main, 2004. (c) Gaiko, N.; Volkmer, A.; Berger, S.; Schaffer, J.; Eggeling, C.; Seidel, C.; Griesinger, C. *Biophys. J.* **2003**, *84*, 313A.
(17) (a) Unruh, J. R.; Gokulrangan, G.; Wilson, G. S.; Johnson C. K. *Photochem. Photobiol.* **2005**, *81*, 682−690. (b) Unruh, J. R.; Gokulrangan, G.; Lushington, G. H.; Johnson C. K.; Wilson, G. S. *Biophys. J.* **2005**, *88*, 3455−3465.
(18) (a) Edman, L.; Mets, Ü.; Rigler, R. *Proc. Natl. Acad. Sci. U.S.A.* **1996**, *93*, 6710−6715. (b) Widengren, J.; Dapprich, J.; Rigler R. *Chem. Phys.* **1997**, *216*, 417−426. (c) Osborne, M. A.; Barnes, C. L.; Balasubramanian, S.; Klenerman, D. *J. Phys. Chem. B* **2001**, *105*, 3120−3126.
(19) Diekmann, S. *J. Mol. Biol.* **1989**, *205*, 787−791.
(20) Case, D. A.; Darden, T. A.; Cheatham, T. E., III.; Simmerling, C. L.; Wang, J.; Duke, R. E.; Luo, R.; Merz, K. M.; Wang, B.; Pearlman, D. A.; Crowley, M.; Brozell, S.; Tsui, V.; Gohlke, H.; Mongan, J.; Hornak, V.; Cui, G.; Beroza, P.; Schafmeister, C.; Caldwell, J. W.; Ross, W. S.; Kollman, P. A. *AMBER 8*; University of California: San Francisco, CA, 2004.
(21) Kale, L.; Skeel, R.; Bhandarkar, M.; Brunner, R.; Gursoy, A.; Krawetz, N.; Phillips, J.; Shinozaki, A.; Varadarajan, K.; Schulten, K. *J. Comput. Phys.* **1999**, *151*, 283−312.
(22) (a) Cornell, W. D.; Cieplak, P.; Bayly, C. I.; Gould, I. R.; Merz, K. M., Jr.; Ferguson, D. M.; Spellmeyer, D. C.; Fox, T.; Caldwell, J. W.; Kollman, P. A. *J. Am. Chem. Soc.* **1995**, *117*, 5179−5197. (b) Wang, J.; Cieplak, P.; Kollman., P. A. *J. Comput. Chem.* **2000**, *21*, 1049−1074.
(23) Wang, J. M.; Wolf, R. M.; Caldwell, J. W.; Kollman, P. A.; Case, D. A. *J. Comput. Chem.* **2004**, *25*, 1157−1174.
(24) (a) Bayly, C. I.; Cieplak, P.; Cornell, W. D.; Kollman, P. A. *J. Phys. Chem.* **1993**, *97*, 10269−10280. (b) Cornell, W. D.; Cieplak, P.; Bayly, C. I.; Kollman, P. A. *J. Am. Chem. Soc.* **1993**, *115*, 9620−9631. (c) Cieplak, P.; Cornell, W. D.; Bayly, C.; Kollman, P. A. *J. Comput. Chem.* **1995**, *16*, 1357−1377.
(25) Frisch, M. J.; Trucks, G. W.; Schlegel, H. B.; Scuseria, G. E.; Robb, M. A.; Cheeseman, J. R.; Montgomery, J. A., Jr.; Vreven, T.; Kudin, K. N.; Burant, J. C.; Millam, J. M.; Iyengar, S. S.; Tomasi, J.; Barone, V.; Mennucci, B.; Cossi, M.; Scalmani, G.; Rega, N.; Petersson, G. A.; Nakatsuji, H.; Hada, M.; Ehara, M.; Toyota, K.; Fukuda, R.; Hasegawa, J.; Ishida, M.; Nakajima, T.; Honda, Y.; Kitao, O.; Nakai, H.; Klene, M.; Li, X.; Knox, J. E.; Hratchian, H. P.; Cross, J. B.; Adamo, C.; Jaramillo, J.; Gomperts, R.; Stratmann, R. E.; Yazyev, O.; Austin, A. J.; Cammi, R.; Pomelli, C.; Ochterski, J. W.; Ayala, P. Y.; Morokuma, K.; Voth, G. A.; Salvador, P.; Dannenberg, J. J.; Zakrzewski, V. G.; Dapprich, S.; Daniels, A. D.; Strain, M. C.; Farkas, O.; Malick, D. K.; Rabuck, A. D.; Raghavachari, K.; Foresman, J. B.; Ortiz, J. V.; Cui, Q.; Baboul, A. G.; Clifford, S.; Cioslowski, J.; Stefanov, B. B.; Liu, G.; Liashenko, A.; Piskorz, P.; Komaromi, I.; Martin, R. L.; Fox, D. J.; Keith, T.; Al-Laham, M. A.; Peng, C. Y.; Nanayakkara, A.; Challacombe, M.; Gill, P. M. W.; Johnson, B.; Chen, W.; Wong, M. W.; Gonzalez, C.; Pople, J. A. *Gaussian 03*, revision C.01, Gaussian, Inc.: Wallingford, CT, 2004.
(26) (a) Miertus, S.; Scrocco, E.; Tomasi, J. *Chem. Phys.* **1981**, *55*, 117−129. (b) Miertus, S.; Tomasi, J. *Chem. Phys.* **1982**, *65*, 239−245. (c) Cossi, M.; Barone, V.; Cammi, R.; Tomasi, J. *Chem. Phys. Lett.* **1996**, *255*, 327−335.
(27) Cavallo, L.; Moore, M. H.; Corrie, J. E. T.; Fraternali, F. *J. Phys. Chem. A* **2004**, *108*, 7744−7751.
(28) Macke, T.; Case, D. A. In *Molecular Modeling of Nucleic Acids*; Leontes, N. B., SantaLucia, J., Jr., Eds.; ACS Symposium Series 683; American Chemical Society: Washington, DC, 1998; pp 379−393.
(29) Jorgensen, W. L.; Chandrasekhar, J.; Madura, J.; Klein, M. L. *J. Chem. Phys.* **1983**, *79*, 926−935.
(30) Babin, V.; Baucom, J.; Darden, T. A.; Sagui, C. *J. Phys. Chem. B* **2006**, *110*, 11571−11581.
(31) (a) Darden, T.; York, D.; Pedersen, L. *J. Chem. Phys.* **1993**, *98*, 10089−10092. (b) Essmann, U.; Perera, L.; Berkowitz, M. L.; Darden, T.; Lee, H.; Pedersen, L. G.; *J. Chem. Phys.* **1995**, *103*, 8577−8593. (c) Toukmaji, A.; Sagui, C.; Board, J.; Darden, T. *J. Chem. Phys.* **2000**, *113*, 10913−10927.
(32) Ryckaert, J.-P.; Ciccotti, G.; Berendsen, H. J. C. *J. Comput. Phys.* **1977**, *23*, 327−341.
(33) Dickerson, R. E.; Bansal, M.; Calladine, C. R.; Diekmann, S.; Hunter, W. N.; Kennard, O.; Lavery, R.; Nelson, H. C. M.; Olson, W. K.; Saenger, W.; Shakked, Z.; Sklenar, H.; Soumpasis, D. M.; Tung, C.-S.; von Kitzing, E.; Wang, A. H.-J.; Zhurkin, V. B. *J. Mol. Biol.* **1989**, *205*, 787−791.
(34) Chuichay, P.; Vladimirov, E.; Jezierski, G.; Rösch, N. *GEV Program*; Technische Universität München: München, Germany, 2006.
(35) (a) Lu, X.-J.; El Hassan, M. A.; Hunter, C. A. *J. Mol. Biol.* **1997**, *273*, 668−680. (b) Lu, X.-J.; Olson, W. K. *Nucleic Acids Res.* **2003**, *31*, 5108−5121.
(36) Gorin, A. A.; Zhurkin, V. B.; Olson, W. K. *J. Mol. Biol.* **1995**, *247*, 34−48.
(37) Hegger, R.; Kantz, H.; Schreiber, T. *CHAOS* **1999**, *9*, 413−435.

BM700549G